J Solid State Electrochem (2012) 16:3355–3362
DOI 10.1007/s10008-012-1779-3

ORIGINAL PAPER

Preparation and performance of polyvinyl alcohol-based activated carbon as electrode material in both aqueous and organic electrolytes

Shuangling Guo · Fang Wang · Hao Chen · He Ren · Rongshun Wang · Xiumei Pan

Received: 15 July 2011 / Revised: 10 April 2012 / Accepted: 17 May 2012 / Published online: 31 May 2012

Abstract Porous carbon materials with high surface area and different pore structure have been successfully prepared by phenolic resin combined with polyvinyl alcohol (PVA) and KOH as activation agents. The surface morphology, structure, and specific surface area of the carbon materials were studied by scanning electron microscopy, X-ray diffraction, and nitrogen sorption measurement, respectively. Furthermore, the effects of specific surface area, pore structure, and electrolyte on electrochemical properties were investigated by galvanostatic charge–discharge measurement. The results show that KOH–PVA-activated carbon materials display specific capacitance as high as 218 $F g^{-1}$ in 30 wt.% KOH aqueous electrolyte, 147 $F g^{-1}$ in 1 M $LiPF_6$/(ethylene carbonate (EC) + dimethyl carbonate) (1:1 *v*/*v*), and 115 $F g^{-1}$ in 1 M Et_3MeNBF_4/propylene carbonate organic electrolyte, respectively. In addition, the carbon materials demonstrate long-term cycle stability, especially the AK3P-0.30 in aqueous electrolyte and the AK2P-0.30 with excellent rate capability in organic electrolyte. These reveal that the existence of a micro-mesoporous structure of activated carbon is beneficial to store energy in an aqueous supercapacitor and broad pore size distribution of activated carbon is favorable to energy storage in an organic supercapacitor. The carbon materials with pore size distribution in different ranges improve the electrochemical performance of supercapacitor in different electrolytes. A new pore-expand agent (PVA combining with KOH) was used to obtain porous carbons with enhanced properties for supercapacitor.

S. Guo · F. Wang · H. Chen · H. Ren · R. Wang · X. Pan (✉)
Faculty of Chemistry, Institute of Functional Material Chemistry, Northeast Normal University,
130024, Changchun, People's Republic of China
e-mail: panxm460@nenu.edu.cn

Keywords Electric double layer capacitor · Activated carbon · Polyvinyl alcohol · Organic electrode

Introduction

With the continuous development of supercapacitor, the safe energy storage device has been applied in many appliances, such as memory backup, intelligent controller, hand-cranked flashlight, and so on. Supercapacitor is divided into electric double-layer capacitor (EDLC) and pseudocapacitor. The EDLC has been attracting increasing interest and attention in researching for its potential in high power output, high energy density applications, excellent reversibility, long cycle life, and safe characteristics. Porous carbon materials have been considered as the most promising materials for a supercapacitor, owing to their large surface area, controlled pore structure, high thermal stability, and relatively low cost [1–12]. The carbon materials with pore size distribution in different ranges improve the electrochemical performance of supercapacitor in different electrolytes. Pore size distribution, surface area, and the size of the electrolyte ions could influence its electrochemical performance significantly [13–15].

The structure of double layers of porous carbons as electrode materials in organic electrolyte might be different from that in aqueous electrolyte [16, 17]. H. Yamada et al. have reported that the porous carbons for EDLC exhibited large specific double-layer capacitance of 120 $F g^{-1}$ in an organic electrolyte of 1 M $LiClO_4$/(PC + dimethoxy ethane) due to their large surface areas and super rate capability resulting from interconnected hierarchical porous structures [18]. L.H. Wang et al. have reported the performance of porous carbons in Et_3MeNBF_4/PC; the results revealed that microporous surface area contributed

to the capacitance much less than external surface [19, 20]. Others have reported the excellent electrochemical performance of porous carbons in KOH aqueous electrolyte, which was ascribed to hierarchical pore structure (abundant micropores and interconnected mesopores with a size of 3–4 nm), high surface area, large pore volume, and well-balanced micro/mesoporosity in the sample [21–23]. Compared with aqueous electrolyte, organic electrolyte exhibits some drawbacks: poorer electrolyte conductivity (typically ~10 mS cm^{-1}) due to their viscous solvent and smaller specific double-layer capacitance (2~10 μF cm^{-2}) [24, 25].

In this study, porous carbons have been prepared from phenolic resin (PF) by adding both PVA and KOH as activation agents. The electrochemical properties of the hierarchical porous carbons were investigated in both aqueous (KOH) and organic ($LiPF_6$/(EC + DMC) and Et_3MeNBF_4/PC) supercapacitor.

Experimental

Preparation of the activated carbon

Phenolic resin was used as precursor to prepare activated carbon; the KOH and PVA were used as pore-expanding agents. The prepared carbon materials were denoted as AK*x*P−*y*, in which A stands for the activated carbon; correspondingly, K and P represent the KOH and the PVA, and *x* represents the mass ratio of KOH/PF; so, *y* is the mass ratio of PVA/PF. The samples AK3, AK3P-0.30, AK3P-0.35, and AK2P-0.30 correspond to the PF and KOH together with PVA (1:3, 1:3:0.30, 1:3:0.35, 1:2:0.30, *w*/*w*/*w*). In the first step, the PVA of the ethanol–water mixture was added to KOH aqueous solution with magnetic stirring; the phenolic resin ethanol solution was then added dropwise to the mixture solution with a dropper. After this step, the mixture was stirred to mud under heated temperature at 90 °C then immediately placed into a stainless steel tube, and the samples were dried at 110 °C for 12 h to reduce the moisture content before inserting them into an electric furnace. The dried samples were put into a horizontal pipe reactor for activation under flowing nitrogen from room temperature up to the target temperature. The samples were activated as follows: (1) temperature-programmed heating with a heating rate of 5 °C min^{-1} from room temperature to 300 °C and kept for 2 h, (2) temperature-programmed heating with a ramping rate of 1 °C min^{-1} from 300 to 750 °C desired activating temperature and kept for 4 h, (3) cooling down to room temperature, and the obtained samples were subsequently transferred into a glass beaker and washed with distilled water; dilute hydrochloric acid was subsequently transferred into the glass beaker and stirred for 6 h. Finally, the activated samples were washed with distilled water until the filtrate appeared neutral and dried to obtain the products.

Characterization

In order to analyze the pore structural properties of the activated carbon materials, nitrogen adsorption–desorption isotherms of the porous carbons were measured with an ASAP2020 autosorb analyzer (Micromeritic, USA) at 77 K. The Brunauer–Emmett–Teller (BET) method was utilized to calculate the specific surface areas (S_{BET}). Total pore volume (V_t), average pore size (D_{av}), and micropore volume (V_{micro}) were calculated from the amount of N_2 adsorbed at a relative pressure (P_r=P/P_0) of 0.1 and 0.95. The distribution of different pore sizes was obtained by the Barrett–Joyner–Halanda (BJH) method. The mesopore volume (V_{meso}) could be obtained by subtracting the micropore volume from the total pore volume. Mesoporosity was defined as the ratio of mesopore volume to the total pore volume [26]. Structural parameters of the activated carbon materials were detected with powder X-ray diffraction (XRD; Rigaku P/max 2200VPC) using Cu Kα radiation. The surface morphologies of porous activated carbons were observed by scanning electron microscopy (SEM; XL 30 ESEM-FEG, FEI Company).

Electrochemical performances of the electrode materials were evaluated using a Button-type capacitor. The working electrodes were prepared by mixing 80 wt.% of activated carbon materials, 10 wt.% of polytetrafluoroethylene (PTFE), and 10 wt.% of acetylene black, in which PTFE was used as a binder and acetylene black was used as a conductive agent. The electrodes were dried at 120 °C under vacuum for 24 h. First, the cells were assembled with two carbon electrodes, 30 wt.% KOH aqueous solutions as the electrolyte, and a glassy paper as a separator. The capacitances of the capacitors were studied by galvanostatic charge–discharge cycle at a current density of 120 mA g^{-1}, and the charge–discharge voltage ranged from 0 to 0.8 V on the electrochemical test instrument (CT2001A Wuhan LAND Electronic Co. Ltd., China). Second, two kinds organic electrolyte of 1 M Et_3MeNBF_4/PC and 1 M $LiPF_6$/(EC + DMC) were used to improve the energy density of the capacitors. The capacitances of the capacitors were studied by galvanostatic charge–discharge cycle at a current density increasing from 60 to 1,000 mA g^{-1}, and the charge–discharge voltage ranged from 0 to 2.4 V on the electrochemical test instrument.

The specific capacitances of the EDLC were calculated according to the following formula: $C_s=4I\Delta t/\Delta Vm$, where C_s (F g^{-1}) is the specific gravimetric capacitance of single electrode, I (A) is the discharge current, Δt (s) is the discharge time, ΔV (V) is the potential change in discharge, and m (g) is the mass of the activated material on both electrodes.

Results and discussion

Porous texture and surface characterizations

The N_2 adsorption–desorption isotherms are shown in Fig. 1a, b. The isotherms of AK3 exhibits type I adsorption isotherms characteristic of microporous carbons. The isotherm for AK2P-0.30 displays increasing N_2 adsorption at relative pressures above 0.4 and hysteresis loops, which is typical of type IV isotherm and indicates that the carbon material contains mesopores. However, the isotherms of AK3P-0.30 and AK3P-0.35 show a capillary condensation knee somewhat less steep than those of AK2P-0.30, presenting type I–IV hybrid-shape isotherms [27], which indicates the presence of mesopores and a multitude of micropores for AK3P-0.30 and AK3P-0.35. The pore size distributions in mesopore range are shown in Fig. 1c. With the BJH method analysis, the AK2P-0.30 shows the uniform pore size distribution at around 3.5–4.5 and 24–32 nm, relatively; AK3P-0.30 and AK3P-0.35 have one small peak at 3.5–4.5 nm, while the AK3 has on a peak. It denotes that the pore size distributions are broadened after the moderate mixture of KOH and PVA.

The BET surface areas and the pore characteristics are illustrated in Table 1. It can be seen that the AK3 possesses the highest surface area and the small average pore size, which confirms that the KOH-activated porous carbon has lots of micropores, in agreement with Fig. 1a. However, the mesoporosity of KOH–PVA-activated porous carbons has been significantly increased. When the ratio of PF/KOH/PVA is 1:3:0.30, the activated carbon material has a relatively higher mesoposity (34 %) and specific surface area (1,759 m^2 g^{-1}), which demonstrates the existence of micro-mesoporous structure for AK3P-0.30. The AK2P-0.30 not only has a quite large average pore size of 4.3 nm but also has a pore size distribution with two distinct peaks in the mesopore range as shown in Table 1 and Fig. 1c. These results further confirm that the addition of KOH and PVA significantly enlarged the pore size.

XRD characterization

The X-ray diffraction patterns of carbon materials are displayed in Fig. 2. There are two broad diffraction peaks at around 2θ=26.30° and 43.75° in each spectrum, corresponding to the diffraction of (002) and (100), respectively. All the carbon materials show preferable graphitic microcrystallites. It is interesting to find that there are no marked diversities in the XRD patterns with the increase of KOH or PVA in Fig. 2. The curves prove that the activation agent's proportion have slightly influenced the microcrystallites of the carbon materials.

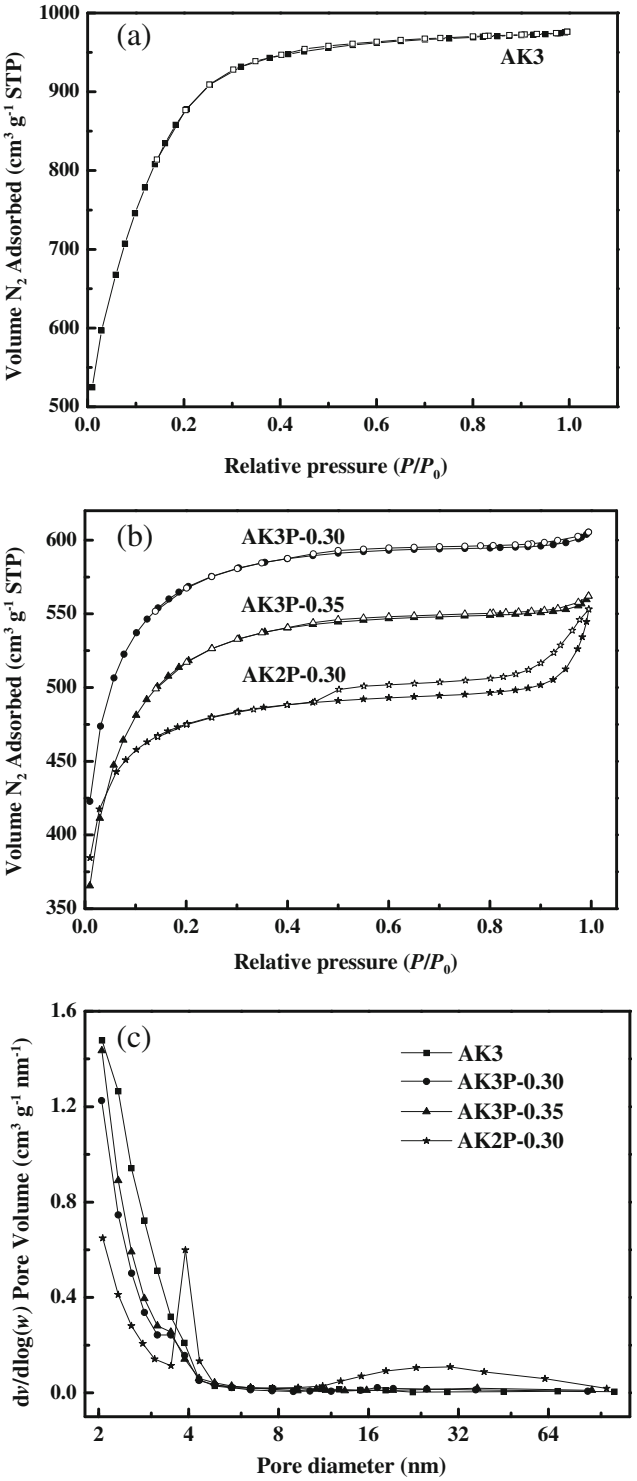

Fig. 1 **a** N_2 adsorption–desorption isotherms of the AK3, **b** N_2 adsorption–desorption isotherms of the AK*x*P−*y*, **c** pore size distributions of the AK3 and AK*x*P−*y*

Morphology characterization

SEM images are conducted to show the surface morphologies of investigated carbon materials (Fig. 3a–d). The

Table 1 Textural characteristics of the AK*x*P–*y*

Samples	S_{BET}, $m^2\ g^{-1}$	D_{BJH}, nm	Total pore volume, $cm^3\ g^{-1}$	V_{micro}, $cm^3\ g^{-1}$	V_{meso}, $cm^3\ g^{-1}$	Mesoporosity, %
AK3	2,218	2.25	1.15	0.87	0.28	24
AK3P-0.30	1,759	2.70	0.93	0.61	0.32	34
AK3P-0.35	1,622	2.70	0.86	0.49	0.37	43
AK2P-0.30	1,452	4.63	0.81	0.56	0.25	31

surface morphologies are clearly different for various activated carbons. The KOH-activated material AK3 has a lot of shallow concave round pores on the surface. As for the KOH–PVA-activated materials AK3P-0.30, AK3P-0.35, and AK2P-0.30, their pores are wider and deeper than that of AK3 relatively. Especially for AK2P-0.30, it has more penetrating pores and wider pore size on the surface. It can be seen that the pore size of AK3P-0.30 is smaller than that of other KOH–PVA-activated materials and that AK3P-0.30 has uniform pore size relatively. Because of the small and uniform pore size, AK3P-0.30 has a larger BET (1,759 $m^2\ g^{-1}$) and more uniform pore size distribution. Therefore, SEM results show that the carbon materials have an apparently honeycomb structure (Fig. 3b–d) in the presence of PVA, which is favorable to ions transport and storage.

Electrochemical performances

Galvanostatic charge–discharge measurements were commonly used to test the performance of capacitors. Figure 4 displays the charge–discharge curves of the AK*x*P–*y*-based EDLC with various current densities, which were obtained ranging 0 to 2.4 V at 60 to 120 mA g^{-1} in 1 M $LiPF_6$/(EC + DMC). A sharp change in voltage at the beginning of the discharge is visible in each sample, which is associated with the equivalent series resistance (ESR) of the EDLC [28].

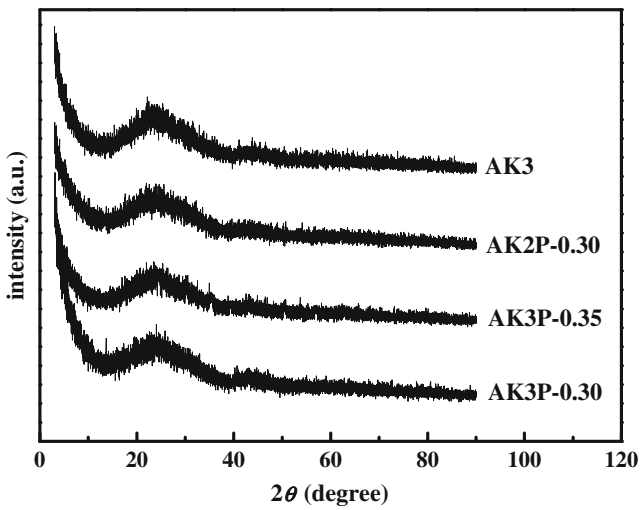

Fig. 2 X-ray diffraction patterns of the AK*x*P–*y*

This potential drop originates mainly from the bulk solution resistance, electrode resistance, and ion migration resistance in the electrode. It is clear that the AK2P-0.30 shows the lowest potential drop in Fig. 4a, which indicates that the ESR of AK2P-0.30 is smaller than that of other electrode materials. Furthermore, AK2P-0.30 has the smallest slope in discharge curves among all electrode materials, which implies that the specific capacitance of AK2P-0.30 is the highest in all carbon materials [29]. This is in agreement with the value of 147 $F\ g^{-1}$ at the current density of 60 mA g^{-1}, which is attributed to the synergy between specific surface area and uniform pore size distribution at around 3.5–4.5 and 24–32 nm and the interconnected porous structure. As shown in Fig. 4b, the specific capacitance of AK2P-0.30 (131 $F\ g^{-1}$) is higher than others and the specific capacitances of the carbon materials are reduced with the increase of current density. Especially, the largest change of specific capacitance among these electrode materials is AK2P-0.30, which is ascribed to the relatively smaller surface areas and fast charge, leading to the Li^+ and PF_6^- ions having some difficulty to penetrate into the inner pores at the current density of 120 mA g^{-1}.

In order to confirm the cycling stability of the carbon materials, galvanostatic charge–discharge experiments were conducted at the current density of 60 mA g^{-1} in 1 M $LiPF_6$/(EC + DMC). Figure 5 shows the dependence of the specific capacitance on the cycle number for all electrode materials. Obviously, the specific capacitance of AK2P-0.30 is higher than others. In addition, the capacity retention of AK2P-0.30 is above 70 % after 1,000 cycles, which exhibits good electrochemical cycle durability.

The effect of KOH's and PVA's content of AK*x*P–*y* carbon materials in 1 M Et_3MeNBF_4/PC at the current density of 60 mA g^{-1} is illustrated in Fig. 6a. The charge–discharge profiles of all electrode materials exhibit almost the isosceles triangle curves, which indicate the simulative capacitor with the performance of electrochemical stability and reversibility. The smallest slope in the discharge curve is observed on AK3, which implies that its specific capacitance is the largest among all electrode materials. This is attributed to the large specific surface area and high surface utilization at low current density. Compared with current density impact, the charge–discharge curves of AK*x*P–*y* carbon materials in 1 M Et_3MeNBF_4/PC at the current density of 120 mA g^{-1} are

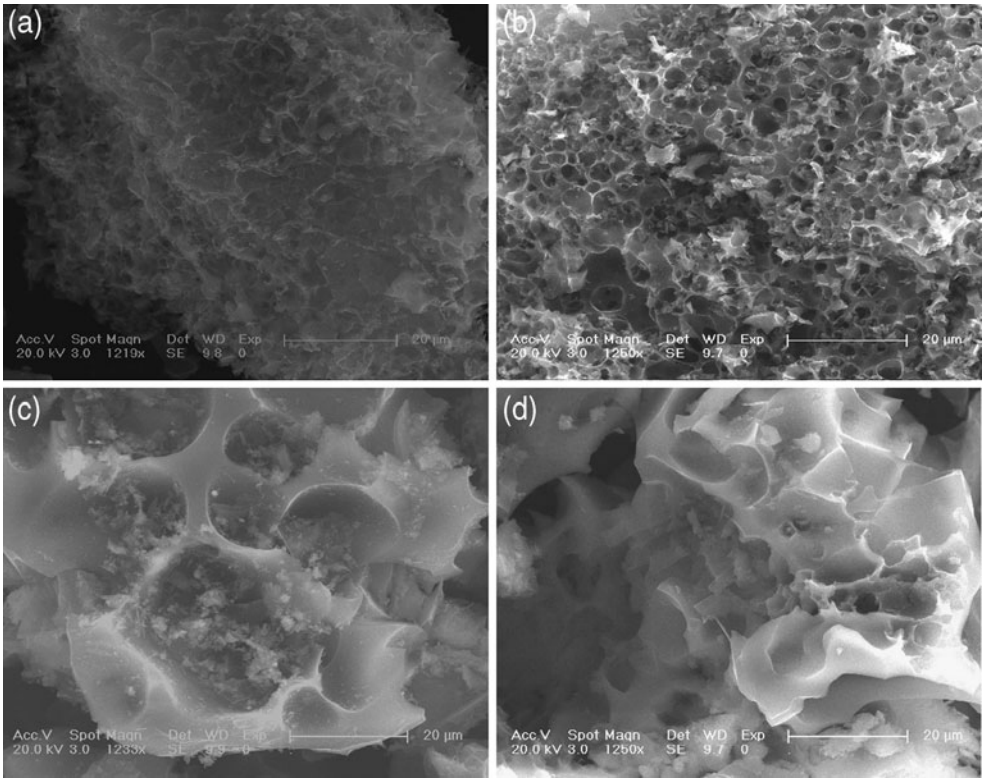

Fig. 3 SEM images of **a** AK3, **b** AK3P-0.30, **c** AK3P-0.35, **d** AK2P-0.30

illustrated in Fig. 6b. The charge–discharge curve of AK3 has a little change, while the AK2P-0.30 has a smaller slope than others. Correspondingly, AK2P-0.30 shows the specific capacitance of 115 Fg^{-1} at the current density of 120 mA g^{-1}, which is higher than the specific capacitance of 98 Fg^{-1} at the current density of 60 mA g^{-1} in 1 M Et_3MeNBF_4/PC, because the AK2P-0.30 has a lot of small micropores in the inner [30]. The discharge capacitances of AK3, AK3P-0.30, and AK3P-0.35 are 109, 104, and 97 Fg^{-1} at the current density of 120 mA g^{-1}, respectively. Obviously, the highest discharge capacitance is observed for AK2P-0.30, which is attributed to the appropriate BET surface area and wide pore size. Therefore, the AK2P-0.30 could be more promising for supercapacitor electrode application owing to its ability to store more energy in 1 M Et_3MeNBF_4/PC at a current density of 120 mA g^{-1}.

The effect of cycle number on specific capacitance in 1 M Et_3MeNBF_4/PC at the current density of 120 mA g^{-1} is shown in Fig. 7. The measured capacity retentions are all above 90 % for all carbon materials after 1,000 cycles, which indicate that the AK*x*P−*y* carbon materials are stable under these long-term charge–discharge cycles. The AK3

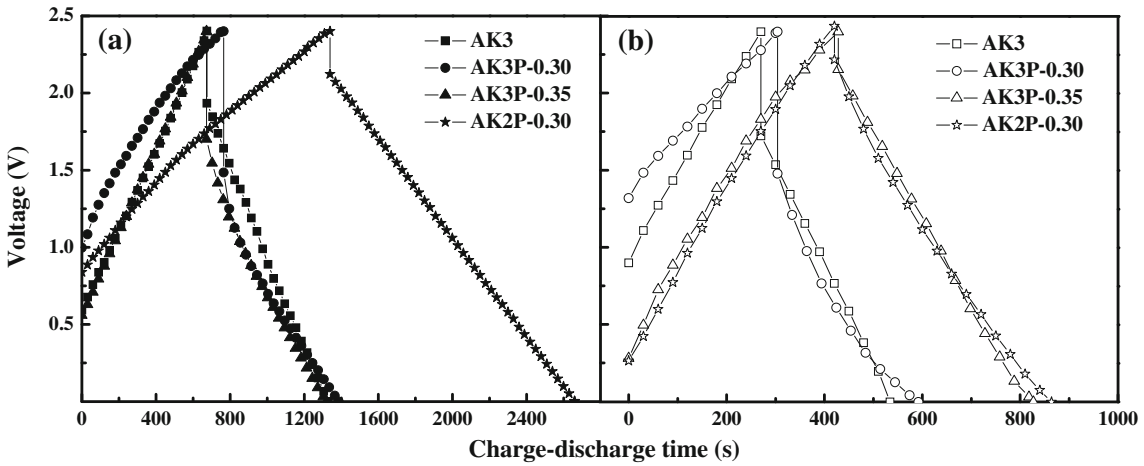

Fig. 4 Galvanostatic charge–discharge curves of the AK*x*P−*y*-based EDLC at a current density of **a** 60 mA g^{-1} and **b** 120 mA g^{-1} in 1 M $LiPF_6$/(EC + DMC) electrolyte

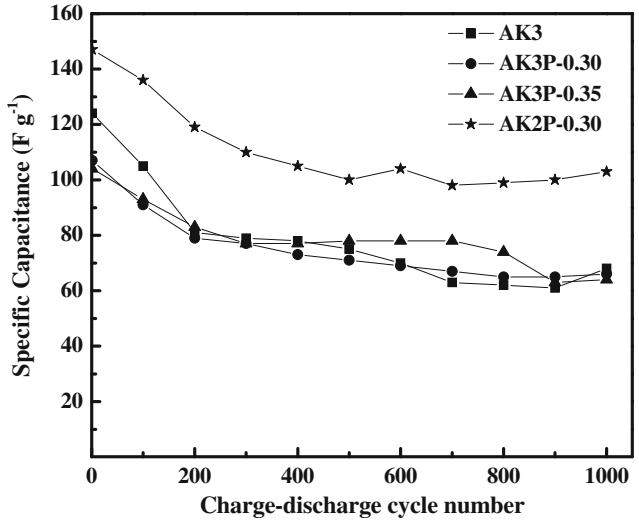

Fig. 5 Variation of specific capacitance with cycle number of the AK*x*P–*y*-based EDLC at a current density of 60 mA g^{-1} in 1 M $LiPF_6$/(EC + DMC) electrolyte

exhibits excellent cycle stability, while the AK2P-0.30 has high specific capacitance and desirable electrochemical reproducibility. It is further confirmed that the AK2P-0.30 displays perfect electrochemical performance at the current density of 120 mA g^{-1} in 1 M Et_3MeNBF_4/PC. Compared with Fig. 5, the AK2P-0.30 has higher specific capacitance in $LiPF_6$/(EC + DMC) [31], while it has better electrochemical cycle stability in Et_3MeNBF_4/PC. It demonstrates that the electrolyte of $LiPF_6$/(EC + DMC) usually has a larger contribution to capacitance; correspondingly, the electrolyte of Et_3MeNBF_4/PC has more contribution to the cycle stability. From the above study, it is confirmed that the AK2P-0.30 possesses superior electrochemical performance in organic electrolyte.

The evolution of the electrical capacitance with the current density was of prime importance to evaluate the potential of carbon materials for high-power applications. Figure 8 depicts the retention rates of specific capacitance for AK2P-0.30 in organic electrolyte. For both electrolytes, specific capacitances decrease with the rise of current densities. The AK2P-0.30 gets a specific capacitance of 92 F g^{-1} at the current density of 1,000 mA g^{-1} in 1 M Et_3MeNBF_4/PC, holding about 80 % of that at 120 mA g^{-1}, suggesting good rate capability; as the current density increases from 60 to 1,000 mA g^{-1} in 1 M $LiPF_6$/(EC + DMC), the specific capacitance of AK2P-0.30 still can keep 106 F g^{-1} with the maintenance ratio above 70 % versus its specific capacitance at 60 mA g^{-1} (147 F g^{-1}), implying appreciable power property. It can be seen that the specific capacitance in $LiPF_6$/(EC + DMC) is higher than that in Et_3MeNBF_4/PC for AK2P-0.30 at the same current density, which is ascribed to its pore size being matching with the ion size of $LiPF_6$/(EC + DMC), thus resulting in higher surface utilization. In order to explain the phenomenon, the solvated ion radiuses of electrolytes were calculated with the Gaussian 03 program [32] by means of the polarizable continunm model. In consideration of the fact that the radius of DMC was larger than that of EC, DMC was chosen as solvent. The solvated cation radiuses for $LiPF_6$/(EC + DMC) and Et_3MeNBF_4/PC were obtained as approximate 0.939 and 1.214 nm, respectively. It is clear that the radius value in $LiPF_6$/(EC + DMC) is smaller than that in Et_3MeNBF_4/PC. Moreover, the solvated anion radiuses for $LiPF_6$/(EC + DMC) and Et_3MeNBF_4/PC are similar (PF_6^-·DMC is approximate 1.137 nm and PF_4^-·PC is approximate 1.106 nm); therefore, there is a higher surface utilization in $LiPF_6$/(EC + DMC). For AK2P-0.30 carbon material, the inner pore ion transport resistance is significantly lowered by the connected mesopores. This facilitates the electrolyte ions to

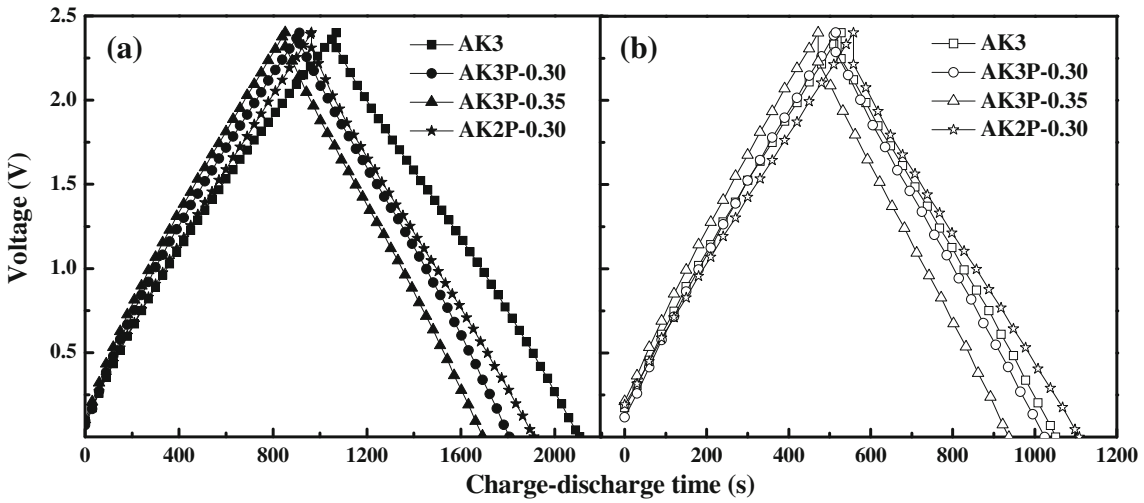

Fig. 6 Galvanostatic charge–discharge curves of the AK*x*P–*y*-based EDLC at a current density of **a** 60 mA g^{-1} and **b** 120 mA g^{-1} in 1 M Et_3MeNBF_4/PC electrolyte

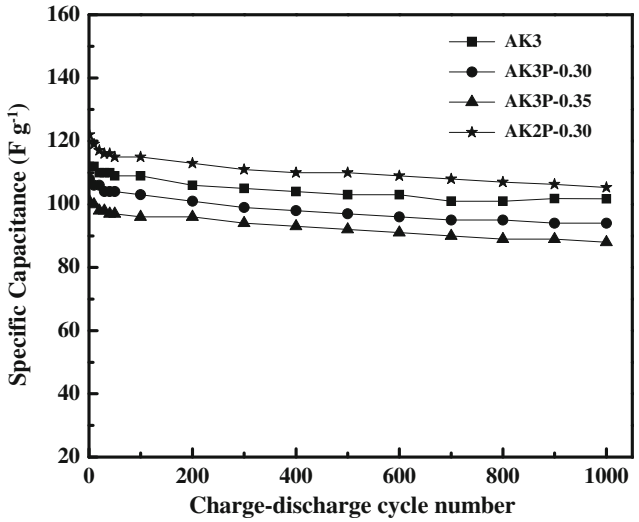

Fig. 7 Variation of specific capacitance with cycle number of the AK*x*P–*y*-based EDLC at a current density of 120 mA g^{-1} in 1 M Et_3MeNBF_4/PC electrolyte

move quickly at high current density and thus gives ideal rate performance. Therefore, AK2P-0.30 may be more promising for supercapacitor electrode application owing to its ability to store more energy in 1 M $LiPF_6$/(EC + DMC) at the current density of 60 mA g^{-1}.

Figure 9 displays the electrochemical performances of the electrode materials and the charge–discharge curves of various carbon materials. The galvanostatic charge–discharge behaviors for the AK3P-0.30 and AK2P-0.30 were performed at the current density of 120 mA g^{-1} between 0 and 0.8 V in 30 wt.% KOH aqueous electrolyte. The slope of the discharge curve for AK3P-0.30 is smaller that that of AK2P-0.30, which demonstrates the highest specific capacitance is observed (218 Fg^{-1}). This can be ascribed to the enhanced specific surface area and porous texture (abundant micropores and interconnected mesopores with the size of 3–4 nm, large pore

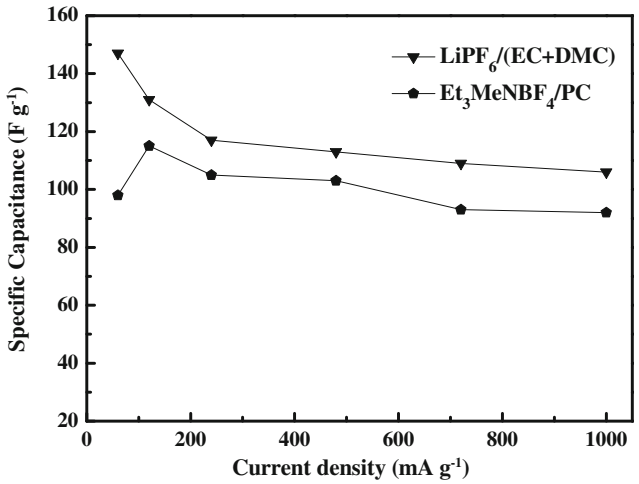

Fig. 8 Specific capacitance as a function of current density for the AK2P-0.30 in organic electrolyte

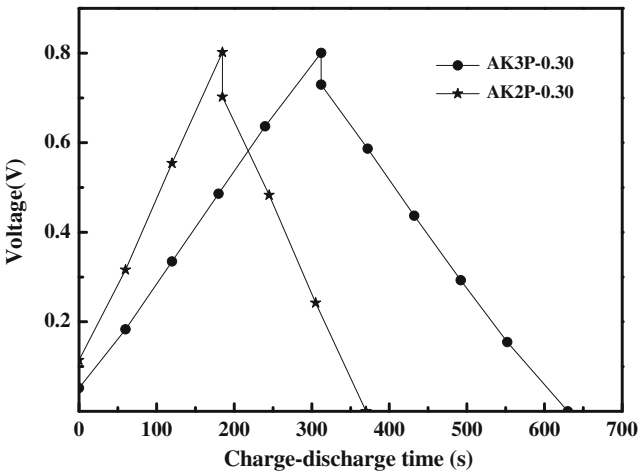

Fig. 9 Galvanostatic charge–discharge curves of the AK3P-0.30 and AK2P-0.30 at a current density of 120 mA g^{-1} in 30 wt.% KOH aqueous electrolyte

volume, and well-balanced micro/mesoporosity in sample) of AK3P-0.30, rendering a larger amount of absorption for electrolyte ions. The discharge capacitance of AK2P-0.30 is 127 F g^{-1}, which is caused by the low volume of pore and surface area. Thus, AK3P-0.30 may be more promising for supercapacitor electrode application, owing to its ability to store more energy in 30 wt.% KOH aqueous solution.

The cycling behaviors of the carbon materials are shown in Fig. 10. The two electrode materials present excellent cycling behavior at the current density of 120 mA g^{-1} in 30 wt.% KOH aqueous electrolyte. Especially, the specific capacitance of AK3P-0.30 is as high as 218 Fg^{-1} and remained after 1,000 cycles. No loss of capacitance of AK3P-0.30 was found during the galvanostatic charge–discharge process, which indicates that the AK3P-0.30 possesses good electrochemical reproducibility.

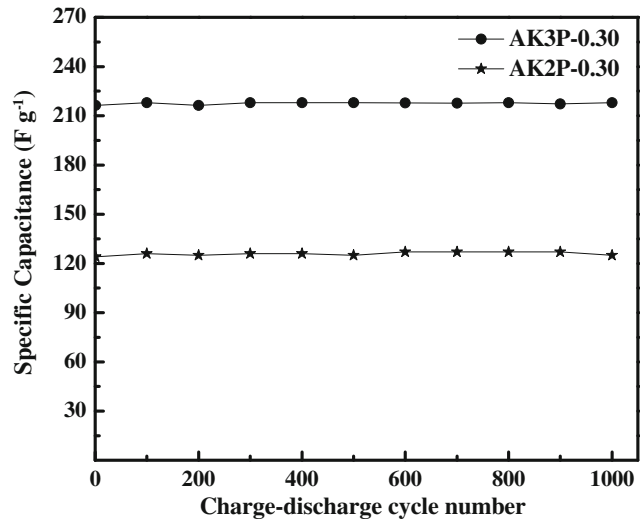

Fig. 10 Variation of specific capacitance with cycle number of the AK3P-0.30 and AK2P-0.30 at a current density of 120 mA g^{-1} in 30 wt.% KOH aqueous electrolyte

Therefore, the AK3P-0.30 carbon material has more potential for supercapacitor electrode application in 30 wt.% KOH aqueous solution; the AK2P-0.30 carbon material could be more promising for supercapacitor electrode application in 1 M $LiPF_6$/(EC + DMC) at a current density of 60 mA g^{-1} and 1 M Et_3MeNBF_4/PC at a current density of 120 mA g^{-1}.

Conclusions

The pore structures and electrochemical performances of the activated carbons as electrode materials in different electrolytes for EDLC, which were prepared from phenolic resin by adding both PVA and KOH as activation agents, were investigated. The present study showed that the PVA and KOH are competitive activation agents for the supercapacitor electrode materials. KOH-activated porous carbon has lots of micropores, while the mesoporosity of KOH–PVA-activated porous carbons has been significantly increased. Specific surface area, pore structure, and electrolyte influenced the specific capacitance for EDLC; therefore, the characterizations of activated carbons were compared in aqueous and organic supercapacitors. In an aqueous supercapacitor, AK3P-0.30 exhibits the best electrochemical performance; it can be ascribed to the existence of a micro-mesoporous structure and an enhanced specific surface area (1,759 m^2 g^{-1}), rendering a larger amount of absorption for electrolyte ions, which is beneficial to store energy in aqueous electrolyte; in an organic supercapacitor, AK2P-0.30 shows the most perfect electrochemical performance, mainly due to the broad pore size distribution at 3.5–4.5 and 24–32 nm, which is favorable to energy storage in organic electrolyte, while the specific capacitance of AK2P-0.30 in $LiPF_6$/(EC + DMC) is higher than that in Et_3MeNBF_4/PC, which is attributed to the pore size of electrode material being matching with the ion size of electrolyte, thus resulting in higher surface utilization of the carbon material. The carbon materials with pore size distribution in different ranges improve the electrochemical performance of a supercapacitor in different electrolytes. By comparison with the KOH-activated porous carbon, this novel activation agent (PVA combined with KOH) seems to be an interesting alternative pathway to obtain porous carbons with enhanced properties for supercapacitor.

Acknowledgments This work is supported by the Training Fund of NENU'S Scientific Innovation Project (NENU-STC07016).

References

1. Kötz R, Carlen M (2000) Electrochim Acta 45:2483–2498
2. Frackowiak E, Béguin F (2001) Carbon 39:937–950
3. Wu FC, Tseng RL, Hu CC, Wang CC (2005) J Power Sources 144:302–309
4. Hu CC, Wang CC, Wu FC, Tseng RL (2007) Electrochim Acta 52:2498–2505
5. Li HQ, Liu RL, Zhao DY, Xia YY (2007) Carbon 45:2628–2635
6. Xu B, Wu F, Chen S, Zhang CZ, Cao GP, Yang YS (2007) Electrochim Acta 52:4595–4598
7. Sevilla M, Álvarez S, Centeno TA, Fuertes AB, Stoeckli F (2007) Electrochim Acta 52:3207–3215
8. Zhu YD, Hu HQ, Li WC, Zhang XY (2006) J Power Sources 162:738–742
9. Xu B, Wu F, Chen RJ, Cao GP, Chen S, Wang GQ, Yang YS (2006) J Power Sources 158:773–778
10. An KH, Kim WS, Park YS, Choi YC, Lee SM, Chung DC, Bae DJ, Lim SC, Lee YH (2001) Adv Mater 13:497–500
11. Xu B, Wu F, Wang F, Chen S, Cao GP, Yang YS (2006) Chin J Chem 24:1505–1508
12. Liu CG, Fang HT, Li F, Liu M, Cheng HM (2006) J Power Sources 160:758–761
13. Qu QT, Wang B, Yang LC, Shi Y, Tian S, Wu YP (2008) Electrochem Commun 10:1652–1655
14. Yang CM, Kim YJ, Endo M, Kanoh H, Yudasaka M, Iijima S, Kaneko K (2007) J Am Chem Soc 129:20–21
15. Lin C, Ritter JA, Popov BN (1999) J Electrochem Soc 146:3639–3643
16. Cericola D, Kötz R, Wokaun A (2011) J Power Sources 196:3114–3118
17. Liu L, Wang W, Zou WY, He BL, Sun ML, Wang M, Xu XF (2010) J Solid State Electrochem 14:2219–2224
18. Yamada H, Moriguchi I, Kudo T (2008) J Power Sources 175:651–656
19. Wang LH, Fujita M, Inagaki M (2006) Electrochim Acta 51:4096–4102
20. Wang LH, Toyoda M, Inagaki M (2008) New Carbon Mater 23:111–115
21. Tian YM, Song Y, Tang ZH, Guo QG, Liu L (2008) J Power Sources 184:675–681
22. Xia KS, Gao QM, Jiang JH, Hu J (2008) Carbon 46:1718–1726
23. Xu B, Wu F, Su YF, Cao GP, Chen S, Zhou ZM, Yang YS (2008) Electrochim Acta 53:7730–7735
24. Ue M, Ida K, Mori S (1994) J Electrochem Soc 141:2989–2996
25. Lozano-Castelló D, Cazorla-Amorós D, Linares-Solano A, Shiraishi S, Kurihara H, Oya A (2003) Carbon 41:1765–1775
26. Zhao JC, Lai CY, Dai Y, Xie JY (2007) Mater Lett 61:4639–4642
27. Ania CO, Pernak J, Stefaniak F, Raymundo-Piñero E, Béguin F (2009) Carbon 47:3158–3166
28. Conway BE (1999) Electrochemical supercapacitors—scientific fundamentals and technological applications. Kluwer Academic, New York
29. Feng ZH, Xue RS, Shao XH (2010) Electrochim Acta 55:7334–7340
30. Zheng ZJ, Gao QM (2011) J Power Sources 196:1615–1619
31. Laheäär A, Kurig H, Jänes A, Lust E (2009) Electrochim Acta 54:4587–4594
32. Klene M, Li X, Knox JE, Hratchian HP, Cross JB, Bakken V, Adamo C, Jaramillo J, Gomperts R, Stratmann RE, Yazyev O, Austin AJ, Cammi R, Pomelli C, Ochterski JW, Ayala PY, Morokuma K, Voth GA, Salvador P, Dannenberg JJ, Zakrzewski VG, Dapprich S, DanielsA D, Strain MC, Farkas O, Malick DK, Rabuck AD, Raghavachari K, Foresman JB, Ortiz JV, Cui Q, Baboul AG, Clifford S, Cioslowski J, Stefanov BB, Liu G, Liashenko A, Piskorz P, Komaromi I, Martin RL, Fox DJ, Keith T, Al-Laham MA, Peng CY, Nanayakkara A, Challacombe M, Gill PMW, Johnson B, Chen W, Wong MW, Gonzalez C, Pople JA (2004) Gaussian 03, revision C.02. Gaussian, Inc, Wallingford